Measurements of the $E2$ resonance effect in pionic atoms

J. J. Reidy and M. Nicholas
Department of Physics and Astronomy, University of Mississippi, University, Mississippi 38677

J. N. Bradbury, P. A. M. Gram, R. L. Hutson, M. Leon, and M. E. Schillaci
Los Alamos National Laboratory, Los Alamos, New Mexico 87545

F. J. Hartmann
Technische Universität München, D-8046 Garching, Federal Republic of Germany

A. R. Kunselman
Department of Physics and Astronomy, University of Wyoming, Laramie, Wyoming 82071
(Received 30 May 1985)

The $E2$ nuclear resonance effect has been studied in the pionic atoms of ^{48}Ti, ^{104}Ru, ^{110}Pd, ^{111,112}Cd, ^{125}Te, and ^{150}Sm. The experimental values of the attenuation for ^{104}Ru, ^{110}Pd, and ^{111,112}Cd agree with the predictions of the theoretical model of Leon. Using the more detailed calculations of Dubach *et al.*, one obtains closer agreement between theory and experiment for ^{150}Sm and ^{48}Ti although in the latter case the difference is still more than two standard deviations. Although the same levels are mixed in ^{125}Te as in ^{104}Ru and ^{110}Pd, the theoretical prediction of the attenuation by Leon is nearly two standard deviations greater than the experimental value. A more precise energy for the second $\frac{5}{2}^+$ state in ^{111}Cd is deduced.

I. INTRODUCTION

Measurements on the x rays emitted by pionic atoms have provided the principal means of studying the zero-energy pion-nucleus interaction. A negative pion incident on a target slows down and is eventually captured by a target atom. The captured pion then cascades down through the pionic atom levels, at first emitting Auger electrons and later pionic x rays. Near the end of the cascade the short-range strong pion-nucleus interaction comes into play. This is reflected in changes in the intensities, energies, and widths of the observed x-ray lines compared to what would be observed in a purely electromagnetic cascade. Compilations of measured pionic x-ray energies and level widths have been given by Poth[1] and Batty.[2] The results of such measurements are reviewed by Hüfner[3] and Batty.[2] These x-ray data are used for determining semiphenomenological optical potentials which give good agreement with most of the x-ray data and are consistent with the optical potentials used to describe low energy pion-nucleus scattering.

However, the strong-interaction information derived from x-ray measurements comes from rather limited regions of Z for each pionic atom level ($1s$ from $Z \lesssim 11$, $2p$ from $8 \lesssim Z \lesssim 33$, $3d$ from $39 \lesssim Z \lesssim 60$, and $4f$ from $Z \gtrsim 67$). This is because, for a given nucleus, the observable x-ray lines terminate rather abruptly at a "last line" as the overlap with the nucleus, and hence the absorption widths, increase. While it would clearly be desirable to test the optical potential for levels with greater overlap with the nucleus, this is not generally possible, so that these levels remain "hidden."

A method to probe a few examples of such hidden levels, the $E2$ nuclear resonance effect, was proposed by Leon.[4] This effect occurs when an atomic deexcitation energy closely matches a nuclear excitation energy and the electric quadrupole coupling induces configuration mixing of the two states. A pion in the (n,l) state (with the nucleus in its ground state) is also partly in an $(n',l-2)$ state (with the nucleus in its excited state); since the $(n',l-2)$ state atomic wave function has a greatly increased overlap with the nucleus, even a very small amount of configuration mixing can result in a significant induced width $\Gamma_{\rm ind}$ in the (n,l) state, which leads to a reduction of the $(n,l)\rightarrow(n-1,l-1)$ x-ray intensity. Measurement of this attenuation allows one to extract information[4,6] about the $(n',l-2)$ pion level. The attenuation may be measured with precision by comparing the intensities of the $(n,l)\rightarrow(n-1,l-1)$ lines in the spectra of two isotopes, one of which possesses the resonance.

The purpose of the present paper is to report the results of such high precision measurements for a number of pionic atoms where the $E2$ nuclear resonance effect is significant. The nuclei studied are ^{48}Ti, ^{104}Ru, ^{110}Pd, ^{111}Cd, ^{112}Cd, ^{125}Te, and ^{150}Sm. We have previously reported results for some of these isotopes[5,7,8] but the present work represents new, more precise and accurate results for all cases. Comparisons are made with theoretical estimates.[4,6] Since they give the most intense lines, we deal exclusively with transitions between "circular" states, for which $l=n-1$.

This work was motivated in part by the persistent discrepancy between an earlier observation and the predictions of the optical potentials for the $3p$ level of pionic Pd

($Z=46$);[5,8] this discrepancy remains even when comparison is made with the more complete calculations of Dubach *et al.*[6] instead of the simpler model of Leon.[4] The $3p$ state is also the lower admixed state in ^{104}Ru and ^{125}Te. The highest Z nucleus where the hadronic contribution to the $1s$ state can be studied is ^{48}Ti, and it has the greatest mixing. A more precise determination of the attenuation would provide a sensitive test for this mixing. Dubach *et al.*[6] have pointed out that pionic ^{150}Sm is potentially very interesting because a precise determination of the attenuation may allow one to distinguish between two nuclear models for ^{150}Sm. Of all the pionic examples of the $E2$ resonance effect ^{111}Cd and ^{112}Cd are the most studied.[5,8] They are important test cases since the lower admixed state is directly observable rather than hidden.

A brief description of the theory for the $E2$ nuclear resonance effect will be presented. Following that the experimental procedure and method of data analysis will be described, the results given, and comparisons made with theory.

II. THEORY

The theoretical description of the $E2$ nuclear resonance effect was first given by Leon[4] and later extended by Dubach *et al.*[6] to include mixing effects due to the strong interaction. We shall present only a summarized description of the theory here, based primarily on the development given by Leon.

Let $|1\rangle$ denote the state consisting of the nucleus in its ground state and the pion in an atomic state (n,l) and $|2\rangle$ the state with the nucleus in an $E2$-excited state and the pion in a lower atomic state $(n',l-2)$. Denoting the quadrupole coupling Hamiltonian by $H'=H'_{\text{strong}}+H'_{\text{em}}$ we can write for the eigenstate $|1'\rangle$

$$|1'\rangle=\sqrt{1-a^2}\,|1\rangle+a\,|2\rangle\ , \tag{1}$$

where a, the admixture coefficient, is given by

$$a=\frac{\langle 2|H'|1\rangle}{\Delta E}\ . \tag{2}$$

The complex energy difference ΔE is

$$\begin{aligned}\Delta E &\equiv E^{2*}_{\text{nuc}}-E_{n',l-2}+E_{n,l}-\tfrac{1}{2}i(\Gamma_{n',l-2}+\Gamma_{n,l})\\ &\equiv\epsilon-i\gamma\ ,\end{aligned} \tag{3}$$

where E^{2*}_{nuc} is the energy of the $E2$-excited nuclear state, $E_{n,l}$ the binding energy of the pion in the n,l pionic atom state, and $\Gamma_{n,l}$ the width of this level. From this admixture of the lower level, the upper atomic level now has an induced width Γ_{ind} which is given by

$$\Gamma_{\text{ind}}=|a|^2\Gamma_{n',l-2}\ . \tag{4}$$

This induced width leads to an attenuation of the x-ray intensity from the n,l state. Conversely, a determination of the x-ray attenuation gives information about the strength of the coupling.

The pionic x-ray transitions which are usually detected are those $E1$ transitions involving circular orbits (maximum l). One determines for a given isotope the intensity ratio of the observed lines,

$$r(Z,A)\equiv\left[\frac{I(n,l\to n-1,l-1)}{I(n+1,l+1\to n,l)}\right]_{Z,A}\ , \tag{5}$$

where $I(n,l\to n-1,l-1)$ represents the measured intensity of the transition between the state n,l and the state $n-1,l-1$ and Z,A represents the isotope. We refer to the isotope where mixing occurs as the "resonant" isotope. For a nonresonant isotope Z,A' one measures the same ratio and then forms the ratio of ratios

$$R=\frac{r(Z,A)}{r(Z,A')}\ . \tag{6}$$

The attenuation A is defined as the complement of R, i.e.,

$$A=1-R\ , \tag{7}$$

and is a direct measure of the induced pion absorption out of the level n,l (to the extent that unresolved noncircular transitions are absent). One can readily show[4] that contours of fixed attenuation are circles in the (ϵ,γ) plane (assuming the mixing matrix element is fixed).

The energies and widths of the pionic atom states are obtained by solving numerically the Klein-Gordon equation[9] with the nuclear Coulomb potential plus the hadronic optical potential. The potential of Seki and Masutani[10] with parameters given in their Table III (the column headed $a-1R$) was chosen. Following Leon,[4] the mixing matrix elements are calculated using nonrelativistic point-nucleus wave functions (electromagnetic contribution only). One then obtains predictions of the attenuation which can be compared with experiment.

There are additional factors which can contribute to the induced width such as nuclear size effects, isomer shifts, nuclear states above the collective quadrupole state, and the inclusion of a p-wave optical potential. Dubach *et al.*[6] have included these.

III. EXPERIMENTAL PROCEDURE AND DATA EVALUATION

These experiments were carried out at the Clinton P. Anderson Meson Physics Facility (LAMPF) using the P^3 and LEP beams. The experimental arrangement was similar to that described in Ref. 5 except that in addition to the 9.6 cm^3 intrinsic Ge detector [with a resolution of $\approx$1.6 keV (FWHM) at 90 keV], some measurements were also made with a 100 cm^3 coaxial Ge(Li) detector [with a resolution of $\sim$2.2 keV (FWHM) at 662 keV]. A spectrum from ^{110}Pd is shown in Fig. 1. Enriched targets of resonant and nonresonant isotopes and natural abundance targets were prepared in 2.5 cm diameter disks, 0.3–2.5 g/cm^2 thick. Each target pair had the same areal density to within 1%, except the Ru targets which differed from each other by 9%. The spectra were analyzed for the line intensities and their statistical errors by using the programs SAMPO (Ref. 12) and LINFIT. This latter code allows one to use a peak shape consisting of a Gaussian line shape convoluted with a Lorentzian line shape and includes exponential tails on either side of the peak.

Using the fitted line intensities and Eqs. (5) and (6), the experimental values of R were determined. These R

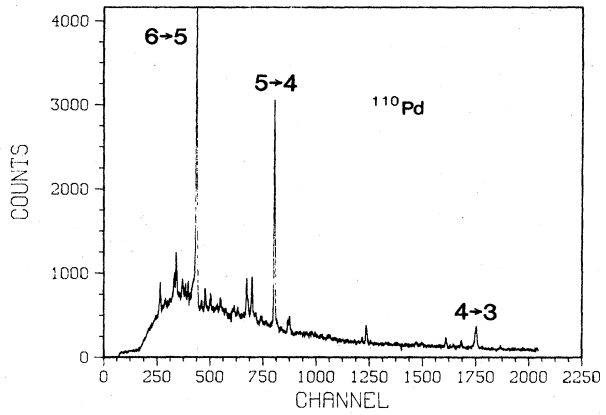

FIG. 1. Pionic x-ray spectrum from ^{110}Pd.

values were then corrected for the fact that the targets were not isotopically pure. In those cases where pure naturally abundant material was used for the "nonresonant" target, corrections for the contribution due to the "resonant" isotope in it also had to be made. For absorptively identical targets no corrections for self-absorption are needed. As a check, the intensities of higher lines were determined in some cases in order to determine whether absorption corrections were necessary. Self-absorption corrections were only important for the Ru targets, where they resulted in a 1% correction to the intensity ratio.

The relevant x-ray lines are listed in Table I. The third through sixth columns give the lines that were analyzed in order to measure the attenuation. For the cadmium isotopes, the reference line is an unresolved doublet, and furthermore two lines, 5→4 and 4→3, exhibit attenuation. The corresponding R values are denoted R_α and R_β, respectively. Special care was taken to investigate the shape of each line to look for interfering gamma-ray lines. In several cases there were weak close-lying gamma-ray lines, but in no case did our analysis indicate the presence of interfering lines in the x-ray peaks.

IV. RESULTS

A. Calculations and measurements

The relevant parameters and calculated results for the induced widths are given in Table II. The second row gives the calculated energy difference of the relevant pionic atom levels using the code MATOM. For the cadmium isotopes, the measured value is used. The third row lists the energy of the nuclear $E2$ excited state. The static quadrupole moment of the excited state is listed in the fourth row; two values are given for ^{110}Pd that correspond to two possible results from Coulomb excitation measurements. The fifth row lists the interaction energy of the excited state quadrupole moment with the lower atomic state; for the odd nuclei which have spin $\frac{1}{2}$, there are two possible orientations with $j=l\pm\frac{1}{2}$, and the values for the antiparallel case are given in brackets. The sum of the second, third, and fifth rows is presented in the sixth row; this corresponds to $\epsilon=\mathrm{Re}\Delta E$ [see Eq. (3)]. The calculated (measured for cadmium) level width of the lower mixed state is listed in the seventh row. The ninth, tenth, and eleventh rows give the contributions to the uncertainty in $\Gamma_{nl}^{\mathrm{ind}}$ due to the uncertainties in $\epsilon,\Gamma_{n'l'}$ and $B(E2\uparrow)$, respectively. (For hidden levels we assume a $\pm10\%$ uncertainty in the shifts and widths.) Finally, the calculated induced width(s) with uncertainties obtained by adding in quadrature the values given in the ninth, tenth, and eleventh rows is given in the twelfth row. Even though there are two values for the induced width for the odd nuclei, the smaller value has little effect on the total induced width.

The attentuation is computed by inserting the induced width into an atomic cascade code PIKACAS which calculates all the $E1$ radiative and Auger transition intensities. The initial distribution used to start the cascade is generally assumed to be statistical. For ^{111,112}Cd, it was not necessary to assume a statistical distribution (see the discussion below).

The results of the measurements and comparisons with theory are presented in Table III. The first column lists the target composition and chemical form used for the

TABLE I. Relevant x-ray lines.

Nucleus	Levels mixed	Attenuated line(s)	Energy (keV)	Reference line(s)	Energy (keV)
$^{48}_{22}$Ti	$3d$-$1s$	3→2	254	4→3	88
$^{104}_{44}$Ru	$4f$-$3p$	4→3	355	5→4	163
$^{110}_{46}$Pd	$4f$-$3p$	4→3	389	5→4	178
$^{111,112}_{48}$Cd	$5g$-$3d$	5→4	194	6→5+8→6	105
		4→3	424		
$^{125}_{52}$Te	$4f$-$3p$	4→3	500	5→4	227
$^{150}_{62}$Sm	$5g$-$4d$	5→4	326	6→5	176

TABLE II. Summary of parameters and calculated results for the induced widths.

	^{48}Ti	^{104}Ru	^{110}Pd[d]	^{111}Cd[g]	^{112}Cd	^{125}Te[g]	^{150}Sm
(1) Mixed levels $nl-n'l'$	$3d$-$1s$	$4f$-$3p$	$4f$-$3p$	$5g$-$3d$	$5g$-$3d$	$4f$-$3p$	$5g$-$4d$
(2) $(E_{nl}-E_{n'l'})_0$ (keV)[a]	−1029.8±37.5	−346.01±0.98	−373.41±1.52	−618.711±0.034[e]	−618.711±0.034[e]	−460.36±3.42	−336.74±0.59
(3) E_{nuc} (keV)	983.512±0.002	358.02±0.07	373.81±0.06	620.2±0.4	617.494±0.097	463.387±0.011	333.95±0.01
(4) Q_{nuc}	0.26±0.08	−0.70±0.08	−0.72±0.14	−0.2±0.2[f]	−0.37±0.04	0.2±0.2[f]	−1.28±0.11
			(−0.47±0.03)				
(5) E_Q (keV)	0.0	−1.45±0.17	−1.71±0.33	−0.15±0.15	−0.285±0.031	−0.69±0.69	−0.90±0.08
			(−1.11±0.08)	(+0.26±0.26)		[2.19±2.19]	
(6) $\epsilon=\text{Re}\Delta E$ (keV)	−46.3±37.5	10.56±1.00	−1.31±1.56	1.34±0.43	−1.502±0.107	2.34±3.49	−3.69±0.60
			(−0.71±1.52)	[1.75±0.48]		[5.22±4.06]	
(7) $-\Gamma_{n'l'}$ (keV)[b]	84.55±8.46	22.28±2.23	25.54±2.55	1.638±0.083[e]	1.638±0.083[e]	38.81±3.88	6.67±0.67
(8) $B(E2\uparrow)$ (e^2b^2)	0.072±0.003	0.834±0.044	0.91±0.06	0.126±0.017	0.484±0.004	0.158±0.005	1.33±0.02
(9) $[\delta\Gamma^{\text{ind}}_{nl}]_{\Delta E}$ (eV)	+0.775	+0.11	+0.04(+0.0)	+ 1.72[+ 0.13]	+ 0.56	+ 0.02[+ 0.006]	+ 0.33
	−0.387	−0.09	−0.09(−0.07)	−0.98[−0.06]	−0.48	−0.08[−0.009]	−0.26
(10) $[\delta\Gamma^{\text{ind}}_{nl}]_{\Gamma_{n'l'}}$ (eV)	+ 0.003	+ 0.01	+ 0.29	0.06[+ 0.10]	+ 0.12	+ 0.14[+ 0.007]	+ 0.01
	−0.010	−0.01	−0.22	−0.06[−0.05]	−0.14	−0.11[−0.066]	−0.02
(11) $[\delta\Gamma^{\text{ind}}_{nl}]_{B(E2)}$ (eV)	+ 0.030	+ 0.06	+ 0.18	+ 0.40[+ 0.03]	+ 0.04	+ 0.04[+ 0.002]	+ 0.03
	−0.030	−0.06	−0.17	−0.50[−0.02]	−0.04	−0.04[−0.002]	−0.02
(12) Γ^{ind}_{nl} (eV)[c]	$0.698^{+0.776}_{-0.388}$	$1.13^{+0.13}_{-0.11}$	$2.62^{+0.34}_{-0.29}$	$2.94^{+1.77}_{-1.10}$	$4.73^{+0.57}_{-0.50}$	1.25±0.15	$1.66^{+0.33}_{-0.26}$
			$(2.65^{+0.34}_{-0.29})$	$[0.19^{+0.17}_{-0.08}]$		$[0.079^{+0.009}_{-0.011}]$	

[a]Uncertainties assumed to be 10% of the strong-interaction energy except as noted.
[b]Uncertainties assumed to be 10% of the width except as noted.
[c]Uncertainties obtained by summing in quadrature the ninth, tenth, and eleventh rows.
[d]See Nuclear Data Sheet for explanation of two possible Q values; values in parentheses correspond to the smaller Q value.
[e]Measured values taken from Ref. 13.
[f]Assumed value from systematics of neighboring nuclei.
[g]Values in square brackets correspond to the quadrupole moment and orbital angular momentum being antiparallel; other values are for the parallel case.

TABLE III. Results of the measurements and comparisons with theory.

Target pair	Lines compared	Present results R_α^{obs}	Present results R_α^{corr}	Present results A_α^{corr} (%)	Previous results A_α (%)[b]	Theory A_α (%)
$^{nat,48}TiO_2$	$\frac{3\to2}{4\to3}$	0.955±0.010	0.941±0.013	5.9±1.3	1.9±3.2	$12.0^{+10.3}_{-6.7}$
$^{nat,104}Ru$	$\frac{4\to3}{5\to4}$	0.913±0.014[a]	0.897±0.016	10.3±1.6	7.2±10.5	10.5±1.0
$^{nat,110}Pd$	$\frac{4\to3}{5\to4}$	0.860±0.007	0.840±0.008	16.0±0.08	19.4±2.8	15.2±1.3
$^{nat,111}CdO$	$\frac{5\to4}{6\to5+8\to6}$	0.908±0.007	0.780±0.007	22.0±0.7	21.8±3.7	21.1±3.2
					20.4±3.6[c]	
	$\frac{4\to3}{6\to5+8\to6}$	R_β=0.922±0.013	0.818±0.014	A_β=18.2±1.4	9.2±5.9	16.4±2.8
					8.6±5.7[c]	
$^{nat,112}CdO$	$\frac{5\to4}{6\to5+8\to6}$	0.624±0.005	0.528±0.006	47.2±0.6	50.5±2.9	46.0±1.7
					44.3±2.2[c]	
	$\frac{4\to3}{6\to5+8\to6}$	R_β=0.710±0.011	0.623±0.012	A_β=37.7±1.2	28.5±5.8	37.4±1.7
					32.2±3.7[c]	
$^{130,125}Te$	$\frac{4\to3}{5\to4}$	0.994±0.012	0.994±0.012	0.6±1.2		2.9±0.3
$^{nat,150}Sm_2O_3$	$\frac{5\to4}{6\to5}$	0.888±0.007	0.868±0.008	13.2±0.8	14.0±3.4	11.1±1.1

[a]Corrected for target thickness and density differences.
[b]From Ref. 8 except as noted.
[c]Reference 14.

"nonresonant" and the resonant measurements. The second column gives the x-ray line designation for the experimental ratio which is given in the third column. The values in the fourth column have been corrected for the isotopic abundances in the resonant and nonresonant targets. The fifth column presents the resultant attenuation values derived from the values in the fourth column. Previous measurements are given for comparison in the sixth column. Calculated results using the widths from Table II are listed in the seventh column. A discussion of each case follows.

B. ^{111,112}Cd test case

All the parameters used in the calculation of the induced width for ^{111}Cd and ^{112}Cd have been measured. In addition, as described in Leon *et al.*[5] and Batty *et al.*,[14] x-ray intensity values for transitions between noncircular orbits have been measured. Consequently, one can constrain the initial distribution. Choosing $(1+al)$ for the shape of the initial distribution at $n=16$, x-ray intensities are calculated as a function of a. X-ray intensity values for transitions originating at $n=6$ or greater will not be affected by variations in the induced width of the $5g$ level; however, the R_α and R_β values will depend on this width. Figures 2(a) and (b) give a plot of R_α and R_β vs the $7\to5/(6\to5+8\to6)$ and $6\to4/(6\to5+8\to6)$ ratios for ^{111}Cd and ^{112}Cd, respectively. The ranges for these latter two ratios determined by Leon *et al.*[5] and Batty *et al.*[14] are indicated. The upper and lower bounds for each R_α and R_β is determined by the range of uncertainty in the induced width. The dashed regions correspond to the measured values. The dotted lines in Fig. 2(b) correspond to the curve obtained by using only *calculated* values for the x-ray parameters in Table II. The calculated values given in Table III are the weighted averages of the values determined with the three separate measured x-ray intensity ratios.

From Fig. 2(a) two features are most striking. The R_α value is nearly independent of the initial distribution and the predicted range of R_α is quite large. From Tabel II we see that this is primarily due to the relatively large uncertainty in the energy values of the nuclear excited state. The excellent agreement between the measured values and calculated values for both ^{111}Cd and ^{112}Cd leads us to deduce that the energy of the nuclear excited state in ^{111}Cd is most likely 620.2±0.2 keV. Conversely, a more precise measurement of this excited state energy could provide a more stringent test of this case, particularly since R_α is relatively insensitive to a.

From Fig. 2(b) we see that the relative uncertainty in the calculated R_α is about a factor of 2 less than for ^{111}Cd, reflecting the more precise energy measurement for

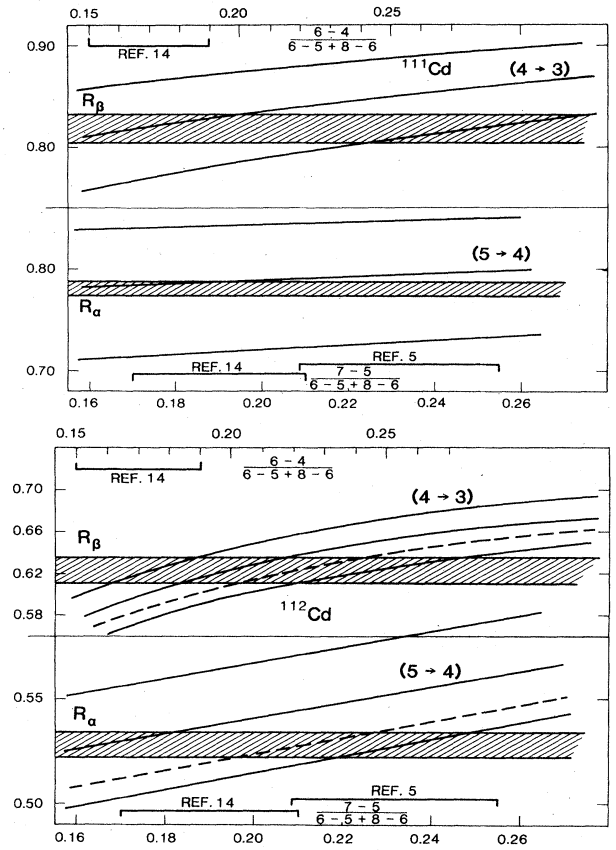

FIG. 2. Attenuation values R_α and R_β vs the $7\rightarrow5/(6\rightarrow5+8\rightarrow6)$ and the $6-4/6\rightarrow5+8-6$ x-ray line intensity ratio for (a) ^{111}Cd and (b) ^{112}Cd.

the nuclear excited state. However, decreasing the uncertainty in the nuclear excited state energy value by a factor of 2 would decrease the uncertainty in R_α only by about 25%. The calculated value of the attenuation in Table III for ^{112}Cd is obtained in a similar fashion as for ^{111}Cd. It is noteworthy that the curve for R_α obtained using *only* calculated values for the parameters gives a weighted attenuation value of $(48.1\pm0.4)\%$. This can be compared with the values reported by Dubach *et al.*[6] of 52.4% using Tauscher[11] parameters (no strong mixing) and 52.59% and 49.44% using Tauscher and Batty parameters, respectively, and including strong mixing.

C. Hidden levels

1. ^{48}Ti

The contour plot for ^{48}Ti is shown in Fig. 3(a). The attenuation values in percent are given for each contour. The measured attenuation range corresponds to the shaded area. The elongated ellipse bounds the region determined from the induced width value in Table II. We see that the major uncertainty in the calculated value is due to a large uncertainty in ϵ. This reflects the assumed 10% uncertainty in the strong interaction contribution to the energy of the $1s$ state (see Table II). The agreement between the calculated and experimental values is marginal for this case. One expects that strong mixing would be significant for this $1s$ state and so the treatment of Dubach *et al.*[6] should be more appropriate. Indeed, they obtained a decrease of the calculated attenuation from a value of 8% to a value of about 2.8% when strong mixing is included. Assuming that a similar decrease would occur if the parameters of Seki and Masutani[10] were used, including strong mixing would then decrease the calculated attenuation value in the present case to approximately 4.5%, in excellent agreement with the experimental value.

2. ^{104}Ru

The contour plot is shown in Fig. 3(b). The striking agreement between the simple theory and experiment is evident. According to Dubach *et al.*,[6] one expects strong mixing to make only a small contribution to the attenuation, and their values of 11% (no strong mixing) and 11.53% and 10.12% (strong mixing) lie within the experimental region.

3. ^{110}Pd

The contour plot for ^{110}Pd is shown in Fig. 3(c). In the past a great deal of effort has gone into trying to reconcile theory and experiment for this case. The theoretical calculations even with strong mixing and unequal neutron and proton distributions gave attenuation values that were too low compared with experiment.[6] However, from Fig. 3(c) we see that even the simple theory now gives excellent agreement with experiment. This is primarily due to the fact that the calculated width of the 3-p state using the parameters of Seki and Masutani[10] is somewhat lower than that calculated by Dubach *et al.*[6] using the Tauscher[11] parameters. From Fig. 3(c) we see that a given change in γ will lead to a larger change in attenuation than a corresponding change in ϵ. Comparison of Table II with the calculations of Dubach *et al.*[6] shows that the values of γ and ϵ used in their work are about 7 keV larger than those used in the present work. Including strong mixing in the present work would increase the theoretical attenuation which would lead only to a marginal improvement in the overlap between theory and experiment.

4. ^{125}Te

The same atomic levels are involved in this case as for ^{104}Ru and ^{110}Pd. The contour plot is presented in Fig. 3(d). For the theoretical region only the parameters in Table II which give the larger induced width are used. Unlike the ^{104}Ru and ^{110}Pd cases, the experimentally determined attenuation value is nearly two standard deviations from the theoretical value. This is the heaviest nucleus that involves the p-wave pion-nucleus interaction on which experiments have been performed, and it is possible that for such a large A the form of the optical potential or the values of the potential parameters are not appropriate. Neutron-proton density distribution differences would play a greater role for ^{125}Te than for lower mass nuclei; this could be another factor leading to the discrepancy between theory and experiment. Dubach *et al.*[6] did not treat odd-A nuclei, so the effect of strong mixing has not been investigated.

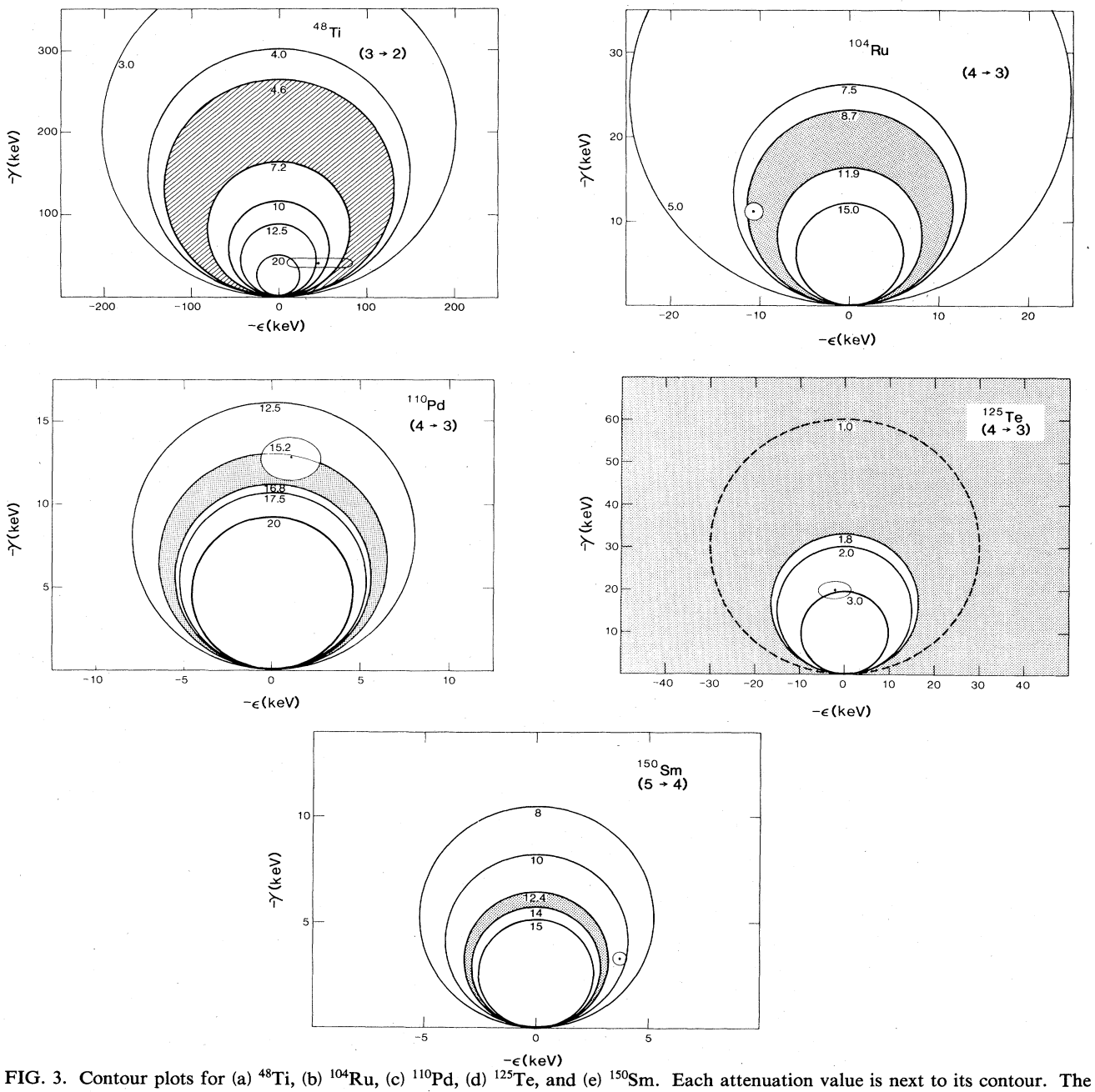

FIG. 3. Contour plots for (a) ^{48}Ti, (b) ^{104}Ru, (c) ^{110}Pd, (d) ^{125}Te, and (e) ^{150}Sm. Each attenuation value is next to its contour. The range of experimental values is represented by the shaded region, and each calculated value with its region of uncertainty is shown by a point and an associated ellipse.

5. *^{150}Sm*

The contour plot for ^{150}Sm is shown in Fig. 3(e). The experimental value for the attenuation is about 2.5 standard deviations larger than the theoretical value. The theoretical value for the attenuation using the simple theory of Leon[4] is nearly the same ($\simeq$11%) whether one uses the parameters of Tauscher[11] or Seki and Masutani.[10] This is not surprising since the mixed atomic states have relatively high n and l values. Dubach *et al.*[6] have shown that the attenuation can be increased to 14.6% if a three-level strong mixing configuration is used. However, this value is still about 1.5 standard deviations from the experimental value. A two-level calculation produces a decrease in the attenuation.

V. CONCLUSIONS

The agreement of the experimental results for the Cd isotopes, where the lower mixed level is observable, with the simple theory is excellent, and indeed for ^{111}Cd the data can be used to deduce a more precise value of the $\frac{5}{2}^+$

excitation energy. The persistent discrepancy between theory and experiment for ^{110}Pd, involving the hidden $3p$ level, now appears to be resolved, and the ^{104}Ru result also shows good agreement. However, ^{125}Te, the last $3p$ case, does have a two standard deviation discrepancy. While the ^{150}Sm value differs from the simple-theory prediction of Leon[4] by more than two standard deviations, the calculation of Dubach *et al.*[6] provides much better agreement. Finally, for the potentially very interesting case of ^{48}Ti, more careful theoretical work is needed for a meaningful comparison.

In summary, the basic $E2$ resonance mechanism is understood, but it is not clear that the effects of the strong interaction are properly included. The present work provides experimental values which should enable one to test more rigorously the inclusion of strong interaction effects.

ACKNOWLEDGMENTS

The encouragement and assistance of the LAMPF staff was most helpful. This work was supported by the U. S. Department of Energy and the National Science Foundation. One of us, F.J.H., would like to thank LAMPF for the kind hospitality he received during his stay.

[1]H. Poth, Phys. Daten, No. 14-1 (1979).
[2]C. J. Batty, Fiz. Elem. Chastis At. Yadra **13**, 164 (1982) [Sov. J. Part. Nucl. **13**, 71 (1982)].
[3]J. Hüfner, Phys. Rep. **21C**, 1 (1975).
[4]M. Leon, Phys. Lett. **50B**, 25 (1974); **53B**, 141 (1974); Nucl. Phys. **A260**, 461 (1976).
[5]M. Leon *et al.*, Phys. Rev. Lett. **37**, 1135 (1976).
[6]J. F. Dubach, E. J. Moniz, and G. D. Nixon, Phys. Rev. C **20**, 725 (1979).
[7]J. N. Bradbury *et al.*, Phys. Rev. Lett. **34**, 303 (1975).
[8]M. Leon *et al.*, Nucl. Phys. **A322**, 397 (1979).
[9]R. Seki (private communication), program MATOM.
[10]R. Seki and K. Masutani, Phys. Rev. C **27**, 2799 (1983).
[11]L. Tauscher, in Proceedings of the International Seminar on π-Meson Nucleus Interactions, Université Louis Pasteur, Strasbourg, France, 1971.
[12]J. T. Routti and S. G. Prussin, Nucl. Instrum. Methods **72**, 125 (1969).
[13]Nucl. Data Sheets **23**, (1978); **41** (1984); **38**, (1983); **27** (1979); **29** (1980); **32** (1981); **18** (1976) (in order of increasing Z).
[14]C. J. Batty *et al.*, Nucl. Phys. **A296**, 361 (1978).